JCI The Journal of Clinical Investigation

Antioxidants stimulate BACH1-dependent tumor angiogenesis

Ting Wang, … , Eckardt Treuter, Martin O. Bergo

J Clin Invest. 2023. https://doi.org/10.1172/JCI169671.

Research In-Press Preview **Angiogenesis**

Graphical abstract

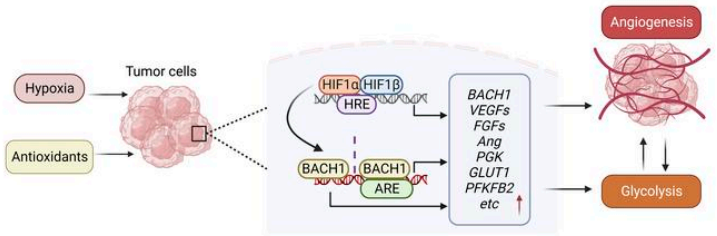

Antioxidants stimulate BACH1-dependent tumor angiogenesis

Ting Wang[1], Yongqiang Dong[2], Zhiqiang Huang[1], Guoqing Zhang[3], Ying Zhao[4,5], Haidong Yao[1], Jianjiang Hu[1], Elin Tüksammel[1], Huan Cai[6], Ning Liang[1,7], Xiufeng Xu[1], Xijie Yang[1], Sarah Schmidt[1], Xi Qiao[1], Susanne Schlisio[8], Staffan Strömblad[1], Hong Qian[6], Changtao Jiang[9,10], Eckardt Treuter[1], and Martin O. Bergo[1,*]

[1] Department of Biosciences and Nutrition, Karolinska Institutet, SE-141 83 Huddinge, Sweden

[2] Department of General Surgery, The First Affiliated Hospital of Zhengzhou University, Zhengzhou 450 052, China

[3] Department of Thoracic Surgery, The First Affiliated Hospital of Zhengzhou University, Zhengzhou 450 052, China

[4] Department of Laboratory Medicine, Karolinska Institutet, SE-171 77 Huddinge, Sweden

[5] Translational Research Center and Center of Allogeneic Stem Cell Transplantation (CAST), Karolinska University Hospital Huddinge, SE-141 86, Stockholm, Sweden

[6] Center for Hematology and Regenerative Medicine, Department of Medicine Huddinge, Karolinska University Hospital, SE-141 86, Huddinge, Sweden

[7] BGI-Shenzhen, Shenzhen 518 083, China

[8] Department of Oncology-Pathology, Karolinska Institutet, SE-171 64 Solna, Sweden

[9] Department of Physiology and Pathophysiology, School of Basic Medical Sciences, Key Laboratory of Molecular Cardiovascular Science, Ministry of Education, Peking University, Beijing 100 191, China

[10] Center of Basic Medical Research, Institute of Medical Innovation and Research, Peking University Third Hospital, Beijing 100 191, China.

* Correspondence: Martin O. Bergo, Professor; Dept. of Biosciences and nutrition, Karolinska Institutet, SE-141 83 Huddinge, Sweden; +46733122224; martin.bergo@ki.se

The authors have declared that no conflict of interest exists.

Abstract

Lung cancer progression relies on angiogenesis, which is a response to hypoxia typically coordinated by hypoxia-inducible transcription factors (HIFs); but growing evidence indicate that transcriptional programs beyond HIFs control tumor angiogenesis. Here we show that the redox-sensitive transcription factor BTB and CNC homology 1 (BACH1) controls the transcription of a broad range of angiogenesis genes. BACH1 is stabilized by lowering reactive oxygen species levels; consequently, angiogenesis gene expression in lung cancer cells, tumor organoids, and xenograft tumors increased substantially following vitamin C and E and *N*-acetylcysteine administration in a BACH1-dependent fashion under normoxia. Moreover, angiogenesis gene expression increased in endogenous BACH1–overexpressing cells and decreased in *BACH1*-knockouts in the absence of antioxidants. BACH1 levels also increased upon hypoxia and following administration of prolyl hydroxylase inhibitors in both *HIF1A*–knockout and wild-type cells. BACH1 was found to be a transcriptional target of HIF1α but BACH1's ability to stimulate angiogenesis gene expression was HIF1α independent. Antioxidants increased tumor vascularity in vivo in a BACH1-dependent fashion, and overexpressing BACH1 rendered tumors sensitive to anti-angiogenesis therapy. BACH1 expression in tumor sections from lung cancer patients correlates with angiogenesis gene and protein expression. We conclude that BACH1 is an oxygen- and redox-sensitive angiogenesis transcription factor.

Introduction

Lung tumor growth and metastasis requires angiogenesis—the formation of new blood vessels (1, 2). Angiogenesis is typically triggered by hypoxia which stabilizes hypoxia-inducible factors (HIFs) including HIF1α and HIF2α which mediate transcription of genes including vascular endothelial growth factors (VEGFs), their receptors (VEGFRs), neuropilin co-receptors (NRPs), epidermal growth factors (EGFs), and angiopoietins (ANGs). Anti-angiogenic drugs targeting these proteins and downstream signaling partners have been developed and approved by the Food and Drug Administration for use in combination with conventional chemotherapy in patients with non-small cell lung cancer (3-7). However, the effects are varied and associated with significant side effects (8, 9). There is also growing evidence that angiogenesis is controlled by transcriptional mechanisms beyond HIFs (10, 11). Thus, identifying new proteins and mechanisms that control tumor angiogenesis, and tumor biomarkers that are associated with heightened sensitivity to anti-angiogenic drugs are worthwhile efforts.

BTB and CNC homology 1 (BACH1) is a redox-sensitive transcription factor that binds antioxidant response elements and is known for its ability to suppress heme oxygenase 1 transcription (12). During oxidative stress, heme released from heme-containing proteins stimulate BACH1 degradation via the ubiquitin ligase FBXO22 (13). Recent studies revealed that lowering oxidative stress in lung cancer cells with *N*-acetylcysteine (NAC), Vitamin E (VitE), or by activating NRF2, reduces reactive oxygen species (ROS) and heme levels, which stabilizes BACH1 and activates transcription of pro-metastatic genes including *HK2* and *GAPDH* (14). Antioxidants thus stimulate aerobic glycolysis and increase local and distant lung cancer metastasis in a BACH1-dependent fashion (14); antioxidants also accelerate malignant melanoma metastasis (15, 16).

Glycolysis is often linked with angiogenesis in tumor progression. HIF1α stimulates angiogenesis which provides oxygen and nutrients to the tumor and upregulates its ability to take up glucose for glycolysis, which in turn provides energy for further angiogenesis and cell proliferation (17). The outcome of BACH1 stabilization following antioxidant administration—i.e., glycolysis and tumor progression—is like that of HIF1α, which is stabilized following hypoxia. We therefore wondered whether BACH1 might also stimulate angiogenesis in response to antioxidants and hypoxia. On one hand, this idea seems counterintuitive, as BACH1 has been suggested to repress angiogenesis (18-20), and vitamin C was found to reduce HIF1α levels and target gene expression in some cancer cell lines (21). On the other hand, BACH1 was found to be associated with VEGFC expression and angio- and lymphangiogenesis in zebrafish (22) and to be increased during hypoxia (23, 24). In this study, we used human and mouse lung cancer cell lines, tumor organoids, and endogenous and xenograft mouse models to address this issue.

Results

BACH1 controls expression of angiogenesis genes in lung tumor organoids and spheroids under normoxia

To explore the role of BACH1 in angiogenesis, we first established 3D cultures of human lung cancer cell lines A549 and H838; tumor organoids from mice with $KRAS^{G12D}$-induced lung cancer; and xenograft tumors from *NSG* mice injected s.c. with A549 cells (Figures 1A and Supplemental Figure 1, A–C). Consistent with previous studies (14), administrating VitC, NAC, and Trolox increased BACH1 protein levels; *BACH1* mRNA levels also increased (Figure 1, B and C and Supplemental Figure 1, D–H). Moreover, the compounds were found to function as antioxidants as H_2O_2 levels decreased and ratios of glutathione (GSH) and glutathione disulfide (GSSG) increased (Supplemental Figure 1I).

VitC, NAC, and Trolox administration increased substantially the expression of angiogenesis genes including VEGFs, VEGF receptors, and NRPs, in the 3D and organoid cultures and xenograft tumors; protein levels of two selected genes, VEGFR2 and NRP2, increased concomitantly (Figure 1, D and E and Supplemental Figure 2, A–J). To determine if BACH1 is functionally involved in angiogenesis gene and protein expression—in the absence of antioxidants—we used CRISPR/CAS9 strategies to increase and decrease endogenous *BACH1* expression in A549 cells (14). Cells with high *BACH1* expression (*BACH1*^{OE}) exhibited increased expression of most tested angiogenesis genes, and higher VEGFR2 and NRP2 protein levels, whereas cells with low *BACH1* expression (*BACH1*$^{-/-}$) exhibited decreased angiogenesis gene and protein expression (Figure 2, A–D and Supplemental Figure 2, K–L). Antioxidant administration and BACH1 manipulations caused similar changes in glycolysis as in angiogenesis gene expression (Supplemental Figure 3, A–F). The ability of VitC to increase angiogenesis gene expression and VEGFR2 protein levels was substantially lower in *BACH1*$^{-/-}$ than in *BACH1*$^{+/+}$ cells, suggesting that BACH1 mediates antioxidant-induced angiogenesis gene expression; similar results were observed with NAC and Trolox and with glycolysis gene expression (Figure 2, E and F and Supplemental Figure 4, A–I).

BACH1-mediated expression of angiogenesis and glycolysis genes correlates with BACH1-dependent epigenetic changes at promoter regions

We next applied Cleavage Under Targets and Tagmentation (CUT&Tag) to analyze the genome-wide chromatin binding of BACH1, along with H3K27ac-marking of transcriptionally active enhancers and promoters. BACH1 bound primarily to promoter regions near transcriptional start sites, and to candidate enhancers within intergenic regions and introns (Figure 3A). The BACH1 CUT&Tag peaks were specific as they highly enriched the BACH1 DNA binding motif, which is also recognized by NFE2, NRF2, BACH2, and AP1 (Figure 3B). Knockout of *BACH1* reduced H3K27ac levels,

both genome-widely and at promoters and enhancers of angiogenesis and glycolysis genes (Figure 3, C–E and Supplemental Figure 5, A–C), suggesting that BACH1 acts directly as a transcriptional activator at these regulatory elements (Supplemental Table 1). Further analyses revealed that basal and VitC-induced expression of members of an extended family of angiogenesis and glycolysis genes was abolished following the knockout of *BACH1* (Figure 3F).

BACH1 expression under normoxia and hypoxia is HIF1α dependent; but BACH1 is sufficient for stimulating angiogenesis gene expression in *HIF1A*-deficient cells

HIF1α stabilization during hypoxia stimulates angiogenesis and glycolysis gene expression and we therefore asked whether increased HIF1α gene or protein levels accompany antioxidant-induced angiogenesis and glycolysis gene expression during normoxia. VitC, NAC, and Trolox increased *HIF1A*, but not *HIF2A*, gene expression in A549 spheroids (Figure 4A). Moreover, the antioxidants dose-dependently increased HIF1α protein levels in A549 and H838 spheroids and lung tumor organoids but had little impact on HIF2α levels (Figure 4B and Supplemental Figure 6, A–C). BACH1 gene expression and protein levels increased during hypoxia (Figure 4C and Supplemental Figure 7A). To explore the mechanism underlying this regulation, we incubated A549 spheroids with the prolyl hydroxylase inhibitors DMOG and FG0041 (25) and found that they increased BACH1 protein levels during normoxia in the absence of other stimuli (Figure 4D); control experiments revealed that HIF1α protein levels increased as expected in response to the two compounds (Figure 4D).

Overexpressing *HIF1A*, but not *HIF2A*, in A549 spheroids also increased BACH1 gene and protein levels under normoxia (Figure 4, E and F and Supplemental Figure 7, B and C). Conversely, basal BACH1 protein levels were markedly lower in *HIF1A*$^{-/-}$ than in control *HIF1A*$^{+/+}$ A549 spheroids under normoxia, and the ability of antioxidants to

increase BACH1 levels under normoxia was abolished in the *HIF1A*$^{-/-}$ cells (Figure 5, A and B and Supplemental Figure 7, D and E). As in the earlier experiments BACH1 levels increased upon hypoxia—to levels exceeding those observed with antioxidants under normoxia; BACH1 levels also tended to increase in *HIF1A*$^{-/-}$ cells upon hypoxia (Figure 5B (lanes 3 and 7) and Supplemental Figure 7, D and E). Incubating *HIF1A*$^{-/-}$ cells with DMOG and FG0041 increased BACH1 protein levels to a similar extent as in *HIF1A*$^{+/+}$ cells (Figure 5C (compare with 4D)). Control experiments revealed that re-expressing exogenous *HIF1A* in the *HIF1A*$^{-/-}$ cells increased both basal and NAC-induced BACH1 levels (Supplemental Figure 7, F and G). We conclude that HIF1α sustains basal BACH1 levels and mediates antioxidant-induced increases in BACH1 levels during normoxia, and that BACH1 gene expression and protein levels increase upon hypoxia in a HIF1α-dependent fashion. The finding that BACH1 protein levels also increase in *HIF1A*$^{-/-}$ cells under hypoxia and in response to hypoxia mimetic drugs, suggest a HIF1α-independent, prolyl hydroxylase–dependent regulation of BACH1.

CUT&Tag analyses revealed that the genome-wide BACH1 chromatin occupancy was lower in *HIF1A*$^{-/-}$ than in *HIF1A*$^{+/+}$ cells, consistent with the downregulation of *BACH1* expression in *HIF1A*$^{-/-}$ cells (Figure 5D). However, overexpressing BACH1 in *HIF1A*$^{-/-}$ cells markedly increased the expression of broad range of angiogenesis and glycolysis genes, demonstrating HIF1α-independent regulation by BACH1 (Figure 5E). CUT&Tag experiments with cells under hypoxia demonstrated increased HIF1α chromatin occupancy both genome-widely (Figure S8A) and at individual gene loci including the *BACH1* gene itself (Supplemental Figure 8, C–F). Transcription factor motif analysis showed enrichment of binding sites for HIF1/2α, KLF, and BACH1 (Supplemental Figure 8B). These results demonstrate that *BACH1* is a transcriptional target of HIF1α but also that BACH1 can stimulate HIF1α-independent angiogenesis and glycolysis gene expression.

BACH1 expression correlates with angiogenesis gene and protein expression in human NSCLC tumors and increases tumor vascularity and the response to anti-VEGF therapy in xenograft tumors

Analyses of Cancer Genome Atlas (TCGA) data revealed that *BACH1* expression in lung cancers correlates with the expression of a broad range of angiogenesis and glycolysis genes; we observed similar results in breast and kidney cancer cohorts (Figures 6A and Supplemental Figure 9, A and B). Immunohistochemical analyses of tumor sections from patients with KRAS-mutant non-small cell lung cancer showed correlations between BACH1 and VEGFA and BACH1 and VEGFR2 (Figure 6, B and C and Supplemental Table 2).

To determine whether antioxidant-mediated BACH1 activation is functionally involved in tumor angiogenesis, we administered NAC and VitC to *NSG* mice harboring *BACH1*$^{+/+}$ and *BACH1*$^{-/-}$ tumors and quantified tumor vascularity with ultrasound analyses. NAC and VitC administration increased tumor vascularity and knockout of BACH1 abolished this effect (Figure 7, A and B and Supplemental Figure 9C). VitE administration produced results that overlapped substantially with those of NAC and VitC, however, they were not statistically significant (Supplemental Figure 9D). Moreover, we argued that increased BACH1 expression might increase the response of tumors to anti-angiogenic therapy. To test this possibility, we injected anti-VEGFR2 antibodies (DC101) into *NSG* mice harboring palpable *BACH1*^{OE} and *BACH1*$^{-/-}$ xenograft tumors. Following an initial growth, *BACH1*^{OE} tumors stopped growing in DC101-injected mice and continued to grow in saline-injected controls; the impact of DC101 on *BACH1*$^{-/-}$ tumors was not significant although the drug tended to reduce a delayed tumor growth increase (Figure 7, C–F and Supplemental Figure 9E). Re-

expressing *BACH1* in the *BACH1*$^{-/-}$ cells restored their sensitivity to DC101 (Supplemental Figure 9, F–H).

Discussion

This study identifies BACH1 as an oxygen- and redox-sensitive transcription factor that controls tumor angiogenesis and vascularity and renders tumors sensitive to antiangiogenic therapy. Our data demonstrate that BACH1 in lung cancer cells is activated during hypoxia and in response to antioxidant administration through both transcriptional and post-translational mechanisms: BACH1 transcription is controlled directly by HIF1α (i.e., BACH1 is a transcriptional target of HIF1α); the post-translational stabilization of BACH1 under hypoxia is HIF1α independent and likely mediated by reduced prolyl hydroxylation-dependent degradation, as BACH1 proteins accumulated substantially in response to prolyl hydroxylation inhibitors in both *HIF1A*$^{+/+}$ and *HIF1A*$^{-/-}$ cells; whereas BACH1 stabilization under reducing conditions—following antioxidant administration—is mediated by reduced heme-dependent degradation, as described (14, 26, 27). Once at high levels, BACH1 acts directly as a transcription factor for a broad range of angiogenesis and glycolysis genes and can regulate these genes independently of HIF1α.

HIF1α gene and protein levels increased following antioxidant administration and was essential for antioxidant-induced increases in BACH1 gene and protein levels. We therefore propose that HIF1α- and BACH1-stimulated angiogenesis and glycolysis contributes to the ability of dietary, pharmacological, and endogenous NRF2-driven antioxidants to accelerate lung tumor progression and metastasis, as described earlier (13, 14, 28).

The finding that ROS-lowering doses of antioxidants increase HIF1α levels was surprising because vitamin C has been shown to reduce HIF1α levels and transcriptional targets in some cancer cells (21). The antioxidant-induced increase in

HIF1α levels was also surprising because increased ROS production from mitochondria during hypoxia is known to increase HIF1α levels by inhibiting hydroxylation-dependent degradation (29, 30). A potential explanation for this discrepancy is that mitochondrial ROS production under hypoxia is a short-term response (hours) (31), whereas the current study analyzed effects after 7 days of antioxidant exposure. Moreover, *HIF1A* gene expression increased following antioxidant administration and likely contributed to the increased protein levels rather than posttranslational hydroxylation-related effects.

The finding that BACH1 stimulates lung tumor angiogenesis and correlates with angiogenesis gene and protein expression in human lung tumors, raises the possibility that BACH1 could be a biomarker for predicting a better outcome from anti-angiogenic therapy. Indeed, anti-VEGFR2 therapy stopped the growth of high-BACH1-expressing tumors but not the growth of low-BACH1 tumors. Future studies should be able to address the efficacy of this possibility in a clinical setting; those studies could potentially extend beyond lung cancer, as we observed correlations between BACH1 and angiogenesis gene expression also in breast and kidney cancer.

Methods

Mice

Animal experiments were approved by the Research Animal Ethics Committees in Gothenburg and Linköping, Sweden. *Kras2*$^{LSL/+}$ mice were on a C57BL/6-129/Sv mixed genetic background (14); controls were always littermates. A low dose of *Cre*-adenovirus (5×10^5 pfu, University of Iowa, Iowa City, IA) were administered intranasally to 6–7-week-old male and female mice. For xenograft experiments, NOD-SCID-gamma mice (*NSG*; NOD.Cg-*Prkdc*^{scid}*Il2rg*^{tm1Wjl}/SzJ, from Charles River) were transplanted subcutaneously with 5×10^5 *BACH1*$^{-/-}$, *BACH1*^{OE}, and *BACH1*$^{-/-}$ *BACH1*^{OE} A549 cells; when tumors were detected (i.e., reached 1–3 mm in size), the

mice were injected intraperitoneally with DC101 (40 mg/kg, BE0060, Bio X Cell) 3 times per week; control mice were injected with PBS. Tumor volume was measured three or five times per week with an electronic caliper and calculated as width^2 × length × ½; tumors were weighed at the endpoint.

Cell culture and regents

The following human cell lines were used: A549 (CRL-7909, ATCC); H838 (CRL-5844, ATCC); ZFN-generated *HIF1A*-knockout (*HIF1α*$^{-/-}$) and control (*HIF1α*$^{+/+}$) A549 cells (CLLS-1014, Sigma-Aldrich); CRISPR-CAS9-generated *BACH1*-knockout (*BACH1*$^{-/-}$) and control (sg*dTomato*, *BACH1*$^{+/+}$) A549 cells (14); and CRISPR-SAM-generated *BACH1*- overexpressing (*BACH1*^{OE}) and control (SAM-sg*Tom*, *BACH1*^{WT}) A549 cells(14). Cell lines tested negative for mycoplasma and were cultured in DMEM low-glucose GlutaMax medium (21885-025, Life Technologies) supplemented with 10% fetal bovine serum (FBS, 26140079, ThermoFisher), 1% non-essential amino acids (NEAA, 11140-035, Life Technologies) and 1% penicillin/streptomycin (15140122, ThermoFisher) in either a normoxic (21% O_2) or hypoxic (1% O_2) cell incubator with 5% CO_2 at 37ºC for 7 days. Reagents were *N*-acetylcysteine (NAC, A7250, Sigma-Aldrich), Vitamin C (VitC, A5960, Sigma-Aldrich), Trolox (238813, Sigma-Aldrich), DMOG (D1070100MG, Frontier Scientific), and FG0041 (Fibrogen, used previously in (32)).

Lentivirus

Cells were transduced with lentiviruses in the presence of polybrene (8 μg/ml, 107689-10G, Sigma-Aldrich) and selected with puromycin (1 μg/ml, A1113803, ThermoFisher) for 48 h, or blasticidin (7.5 μg/ml, A1113903, ThermoFisher) for 7 days. Lentiviruses (pLV-EGFP-CMV-FLAG/gene) overexpressing (OE) *BACH1*, *HIF1A*, *EPAS1*, and *EGFP* (control) were produced by VectorBuilder.

Mouse lung tumor organoids

Mouse lung tumor tissue was dissected into ~1 mm^3 fragments with sterile scissors and incubated at 37ºC for 1 h in Eppendorf tubes with 1 ml digestion medium (Advanced DMEM/F-12, 10% FBS, Glutamine, HEPES, and penicillin/streptomycin (ThermoFisher) supplemented with Collagenase type IV (100 mg, Sigma-Aldrich) and Dispase II (20 mg, ThermoFisher)). The cells were pelleted by centrifugation for 5 min at 200 × *g* and 4ºC and resuspended in 150 µl Growth Factor Reduced Matrigel (356231, Corning). Domes of 50 µl cell/Matrigel suspension was pipetted into wells of a pre-warmed 24-well plate which were allowed to solidify for 10 min at 37ºC. Pre-warmed growth medium (same as digestion medium without Collagenase and Dispase) supplemented with 10 µM RHO Kinase inhibitor (Rocki, Y-27632, Sigma-Aldrich), Insulin-Transferrin-Selenium Supplement (Sigma-Aldrich), and TGFβR inhibitor (A83-01, ThermoFisher) was added to the wells and the plate was incubated at 37ºC.

Spheroid (3D) culture

Cultured human cancer cells were trypsinized, counted and mixed with Matrigel (356231, Corning). Domes of 25 µl cell/Matrigel suspension was pipetted into wells of a pre-warmed 24-well plate which were allowed to solidify for 10 min at 37ºC. The cells were then cultured as described for organoids.

ROS measurements

Cells were incubated with NAC and VitC for 7 days and seeded in white 96-well plates (5000 cells/well). ROS were measured with the ROS-Glo-H2O2 assay (G8820, Promega). The ratio of GSH/GSSG was determined with the GSH/GSSG-Glo assay (V6611, Promega). Fluorescence was recorded with a Synergy multimode reader (BioTek).

TCGA data analysis

For analysis of data in The Cancer Genome Atlas (TCGA), BACH1 expression data (RNA Seq V2 RPKM-UQ) from 3372 publicly available cases including 1132 lung, 1220 breast, and 1020 kidney cancer were downloaded from the GDC API using TCGA biolinks R package. For each cancer type, cases were sorted into a high *BACH1* expression group (25% of the samples with the highest expression) and a low expression group (25% samples with the lowest expression). The expression of angiogenic genes were compared between high *BACH1* and low *BACH1* groups by two-tailed *t* test. Angiogenic genes with $P < 0.05$ were retained and their correlation with *BACH1* were calculated using Pearson correlation coefficient.

Immunohistochemistry

Ethical approval (ZBMT001) was obtained from the Ethics Committee of the first affiliated hospital of Zhengzhou university, and all experiments were performed according to the Helsinki Declaration. Human *KRAS*-mutant non-small cell lung cancer (NSCLC) biopsy sections and linked clinical data (Table S2) were obtained from the Zhengzhou university Cancer Biobank and written informed content was signed by 20 NSCLC patients at the time of original biopsy sample collection. Samples were dehydrated, formalin-fixed, and paraffin-embedded, and 5-μm serial sections were mounted on glass slides. The sections were incubated with primary antibodies recognizing BACH1 (sc-271211, Santa Cruz Biotechnology, 1:200), VEGFA (sc-7269, Santa Cruz Biotechnology, 1:200), and VEGFR2 (sc-6251, Santa Cruz Biotechnology, 1:200) at 4 °C overnight, followed by incubation with horseradish peroxidase-conjugated secondary antibodies (Zhong-shan Golden Bridge) for 1 hour. The sections were stained with 3,3'-diaminobenzidine and hematoxylin. The stained sections were then scanned in a Panoramic Confocal (3DHistech, Hungary). Quantification of BACH1, VEGFA, and VEGFR2 staining intensity was performed with Aipathwell digital pathology AI-based image analysis software. Each sample was

assigned a score based on modified H-scores [H-scores = $\sum$ (pi × i) = (percentage of weak intensity × 1) + (percentage of moderate intensity × 2) + (percentage of strong intensity × 3)](33-36).

Cleavage Under Targets and Tagmentation (CUT&Tag) chromatin profiling

We used CUT&Tag to assess the genome-wide chromatin enrichment of BACH1 and H3K27ac in A549 3D spheroids. CUT&Tag was performed on 10^5 cells from 3D spheroid cultures essentially as described(37) using digitonin (Sigma, D5628) for cell permeabilization and concanavalin A–coated magnetic beads (Bangs Laboratories, BP531) for immobilization. Two biological replicates were used for all experiments. Primary antibodies were H3K27ac (Abcam, ab4729), BACH1 (R&D, AF5776), and HIF1α (Novus Biologicals, NB100-134); secondary antibodies were anti-goat (Sigma, SAB3700280) and anti-rabbit (EpiCypher, 13-0047). Samples were incubated with pAG-Tn5 (EpiCypher, 15-1117) for 1 h. After tagmentation, the cleaved DNA was extracted using the DNA Clean & Concentrator-5 Kit (Zymo Research, D4013). IDT primers (Illumina, 20027213) and PCR enzyme mix (NEB, M0541S) were used for library preparation, and AMPure bead (Beckman Coulter, A63881) was used for PCR cleanup. DNA concentration was measured by Qubit (Invitrogen, Q32851). Library samples were sequenced on NextSeq 2000 (PE100) platform (BEA, Karolinska Institutet) using pair-ended output.

CUT&Tag sequencing data analysis

Sequencing files (FASTQ) were aligned to the GRCh37/hg19 human reference genome using Bowtie2(38). Peak calling was computed via MACS2(39). The sequencing tags (SAM) and peak file (BED) were imported to the HOMER for statistical analysis(40). BedGraph files were imported into IGV software for data visualization. 10^7 total tags were used as normalization factor to compare treatments/groups. Motif analysis was done with HOMER (findMotifs.pl). Peak

coverage was calculated with HOMER tool Histograms Tag (annotatePeaks.pl) and visualized in R. The BACH1 peak distribution was based on the HOMER annotation file. Changes in individual peak tags (percentage) were calculated from normalized HOMER output data. The HIF1α genome-wide heatmap was calculated via Deeptools (41).

Reverse transcription quantitative PCR (RT-qPCR)

Cell recovery solution (DLW354253, Sigma-Aldrich) was used to isolate cells from Matrigel. RNA was isolated with the RNeasy Plus Mini kit (74136, Qiagen) and cDNA was synthesized with the iScript cDNA synthesis kit (170-889, Bio-Rad). Gene expression was analyzed with SYBR Green Master Mix (KCQS00, Sigma-Aldrich) on a CFX384 Real-Time System (Biorad) using predesigned KiCqStart SYBR-Green Primers (all from Sigma-Adrich): *BACH1* (H_*BACH1*_1), *HIF1A* (H_*HIF1A*_1), *HIF2A* (H_*EPAS1*_1), *VEGFA* (H_*VEGFA*_1), *VEGFB* (H_*VEGFB*_1), *VEGFC* (H_*VEGFC*_1), *VEGFD* (H_*FIGF*_1), *VEGFR1* (H_*FLT1*_1), *VEGFR2* (H_*KDR*_1), *VEGFR3* (H_*FLT4*_1), *NRP1* (H_*NRP1*_1), *NRP2* (H_*NRP2*_1), *GLUT1* (H_*SLC2A1*_1), *GLUT3* (H_*SLC2A3*_1), *HK1* (H_*HK1*_1), *HK2* (H_*HK2*_1), *PGK1* (H_*PGK1*_1), *PDK1* (H_*PDK1*_1), *PFKP* (H_*PFKP*_1), *PFKFB2* (H_*PFKFB2*_1), *PFKFB3* (H_*PFKFB3*_1), *PKM2* (H_*PKM2*_1), *PKLR* (H_*PKLR*_1), *LDHA* (H_*LDHA*_1), *FGF2* (H_*FGF2*_1), *FGF7* (H_*FGF7*_1), *FGF9* (H_*FGF9*_1), *FGFR1* (H_*FGFR1*_1), *FGFR2* (H_*FGFR2*_1), *FGFR3* (H_*FGFR3*_1), *FGFR4* (H_*FGFR4*_1), *FGFR1OP* (H_*FGFR1OP*_1), *EGF* (H_*EGF*_1), *EGFR* (H_*EGFR*_1), *EGFL7* (H_*EGFL7*_1), *EFNA5* (H_*EFNA5*_1), *ANGPT1* (H_*ANGPT1*_1), *ANGPT2* (H_*ANGPT2*_1), *ANGPTL1* (H_*ANGPTL1*_1), *ANGPTL2* (H_*ANGPTL2*_1), *ANGPTL4* (H_*ANGPTL4*_1), *Bach1* (M_*Bach*_1), *Vegfa* (M_*Vegfa*_1), *Vegfb* (M_*Vegfb*_1), *Vegfd* (M_*Figf*_1), *Vegfr1* (M_*Flt1*_1), *Vegfr2* (M_*Kdr*_1), *Vegfr3* (M_*Flt4*_1), *Nrp1* (M_*Nrp1*_1), *Nrp2* (M_*Nrp2*_1), *Hk1* (M_*Hk1*_1), *Hk2* (M_*Hk2*_1), *Pgk1* (M_*Pgk1*_1), *Pdk1* (M_*Pdk1*_1), *Pfkp* (M_*Pfkp*_1), *Pfkfb2* (M_*Pfkfb2*_1), *Pfkfb3*

(M_*Pfkfb3*_1), *Pkm2* (M_*Pkm2*_1), *Pklr* (M_*Pklr*_1); *ACTIN* (H_*ACTB*_1), *Actin* (M_*Actb*_1) was the reference gene.

Western Blotting

Cell recovery solution (DLW354253, Sigma-Aldrich) was used to isolate cells from Matrigel. Cells were lysed in Laemmli buffer supplemented with β-mercaptoethanol. Equal amounts of proteins were resolved on 4–20% or 10% Mini-PROTEAN TGX Stain-Free gels (456-8036, Bio-Rad) and electro-transferred onto nitrocellulose membranes (0.2 µm, 1704158; Bio-Rad). The membranes were blocked with 5% milk in TBST and incubated with primary antibodies overnight and secondary antibodies for 1 h at room temperature. Primary antibodies were BACH1 (sc-271211, Santa Cruz Biotechnology, 1:1000), VEGFR2 (sc-6251, Santa Cruz Biotechnology, 1:200), NRP2 (sc-13117, Santa Cruz Biotechnology, 1:200), ACTIN (Sigma-Aldrich, A2228, 1:1000), H3K27ac (ab4729, Abcam, 1:2000), HIF1α (#14179, #3716, Cell Signaling, 1:1000), and HIF2α (#PA1-16510, Invitrogen, 1:1000). Secondary antibodies were Rhodamine (TRITC) AffiniPure Goat Anti-Mouse IgG (H+L) (115-025-003, 1:10 000) and Peroxidase AffiniPure Goat Anti-Rabbit IgG (H+L) (111-035-003, 1:10 000) from Jackson Immunoresearch laboratories. Western ECL substrate (1705061, Bio-Rad) was used for protein band detection with the ChemiDoc Touch Imaging system (1708370, Bio-Rad). Band densities were quantified with Image Lab Software.

High-frequency ultrasound imaging

NSG mice were subcutaneously transplanted with 5 × 10^5 *BACH1*$^{-/-}$ and *BACH1*$^{+/+}$ A549 cells and received NAC (1 g/l) or VitC (3.47 g/l) in the drinking water, or VitE (DL-α-tocopheryl acetate) in the chow (Lantmännen) at a dose of 0.5 g/kg chow (61.5 mg/kg body weight), calculated from an observed daily food intake (28). Ultrasound (US) imaging of tumors was performed on a Vevo LAZR-X Imaging Station (VisualSonics, Inc., Toronto, Canada) using a high-frequency ultrasound probe

MX250 (15–30 MHz, 75 µm image axial resolution). Mice were anesthetized with 1.5% isoflurane and medical air flow of 2 l/min during the imaging process; hair over the imaged area was removed using a depilatory cream; and US gel (Parker Laboratories) was applied over the region of interest. Tumor size quantification was performed using 18 MHz B-mode. 3D images were acquired via a 3D acquisition motor scanned along the vertical axis. 3D volumetric quantification was performed be integrating multiple two-dimensional US images. Nonlinear contrast imaging was acquired at 18 MHz frequency, 10% power, 30 dB contrast gain, and 20/sec frame rate—immediately after an intravenous bolus injection of 50 µl non-targeting microbubbles (2×10^9/ml, VevoMicroMarker Contrast Agent, VisualSonics). Tumor perfusion/vascularity (peak enhancement) was quantified with VevoCQ Software (VisualSonics).

Data availability

Graphical abstract was created with BioRender.com. Sequence data from the CUT&Tag experiments and have been deposited at NCBI Gene Expression Omnibus (GEO) with accession number GSE209958 and reviewer token ajqlaqcktfatxaz.

Statistics

Data are shown as mean ± SEM. Graphpad Prism software v.8 was used for statistical analyses; we used two-way ANOVA for tumor volume; unpaired *t* test when comparing only two groups; and one-way ANOVA followed by Tukey's test for all other comparisons. The relationship between BACH1 and VEGFA and VEGFR2 expression was analyzed with Pearson's correlation test. *P* less than 0.05 was considered significant difference. Experiments were repeated 2–4 times unless stated otherwise; n indicates biological replicates.

Study approval

Animal experiments were approved by the Research Animal Ethics Committees in Gothenburg and Linköping, Sweden. Analyses of human tissues were approved by

the Ethics Committee of the first affiliated hospital of Zhengzhou university, and human experiments were performed according to the Helsinki Declaration. Human tissues were de-identified, and all patients provided written informed consent.

Author contributions

T.W. designed the study, performed experiments, interpreted data, made figures, and wrote the manuscript; Y.Q.D. and G.Q.Z. performed and analyzed human NSCLC experiments; Z.H., N.L., and Eckardt.T. designed, performed, and analyzed CUT&Tag experiments; H.D.Y. provided advice and performed mouse experiments; Elin.T., H.C., X.J.Y., and Sarah.S. performed mouse experiments; C.T.J. designed experiments; Y.Z. performed and analyzed photoacoustic imaging experiments; X.Q., J.J.H., and Staffan.S. provided technical support; X.X. and Susanne.S. provided advice and reagents; H.Q. supervised and provided infrastructure and advice; M.O.B. conceived the study, interpreted data, supervised, provided funding, and wrote the manuscript. All authors read and commented on the manuscript.

Acknowledgments

We thank Hui Wan (Department of Biosciences and Nutrition, Karolinska Institutet, Huddinge, Sweden) for analyzing TCGA data. The study was supported by grants from the Knut and Alice Wallenberg Foundation, Cancer Research KI, The Sjöberg Foundation, Center for Innovative Medicine, the Swedish Cancer Society, and Medical Research Council (to M.O.B). T.W. was partly supported by the China Scholarship Council. Z.H. was supported by a Lilly Young Investigator Award (97081) from the European Foundation for the Study of Diabetes (EFSD). E.T. was supported by grants from the Swedish Research Council (2020-01150), the Swedish Cancer Society (2018/636) and the Novo Nordisk Foundation (NNF20OC006367200 and NNF21OC0070256).

References

1. Folkman J. Angiogenesis in cancer, vascular, rheumatoid and other disease. *Nat Med.* 1995;1(1):27-31.
2. Yamazaki K, et al. Tumor angiogenesis in human lung adenocarcinoma. *Cancer.* 1994;74(8):2245-2250.
3. Sandler A, et al. Paclitaxel-carboplatin alone or with bevacizumab for non-small-cell lung cancer. *N Engl J Med.* 2006;355(24):2542-2550.
4. Sandler A, et al. Treatment outcomes by tumor histology in Eastern Cooperative Group Study E4599 of bevacizumab with paclitaxel/carboplatin for advanced non-small cell lung cancer. *J Thorac Oncol.* 2010;5(9):1416-1423.
5. Reck M, et al. Phase III trial of cisplatin plus gemcitabine with either placebo or bevacizumab as first-line therapy for nonsquamous non-small-cell lung cancer: AVAil. *J Clin Oncol.* 2009;27(8):1227-1234.
6. Tassinari D, et al. Bevacizumab in the treatment of advanced, non-squamous non-small cell lung cancer: an evidence-based approach. *Oncology.* 2011;80(5-6):350-358.
7. Garon EB, et al. Ramucirumab plus docetaxel versus placebo plus docetaxel for second-line treatment of stage IV non-small-cell lung cancer after disease progression on platinum-based therapy (REVEL): a multicentre, double-blind, randomised phase 3 trial. *Lancet.* 2014;384(9944):665-673.
8. Wang S, et al. Are VEGFR-TKIs effective or safe for patients with advanced non-small cell lung cancer? *Oncotarget.* 2015;6(20):18206-18223.
9. Pilotto S, et al. Anti-angiogenic drugs and biomarkers in non-small-cell lung cancer: a 'hard days night'. *Curr Pharm Des.* 2014;20(24):3958-3972.
10. Choudhry H, Harris AL. Advances in Hypoxia-Inducible Factor Biology. *Cell Metab.* 2018;27(2):281-298.

11. Weis SM，Cheresh DA. Tumor angiogenesis: molecular pathways and therapeutic targets. *Nat Med.* 2011;17(11):1359-1370.
12. Sun J, et al. Hemoprotein Bach1 regulates enhancer availability of heme oxygenase-1 gene. *Embo j.* 2002;21(19):5216-5224.
13. Lignitto L, et al. Nrf2 Activation Promotes Lung Cancer Metastasis by Inhibiting the Degradation of Bach1. *Cell.* 2019;178(2):316-329.e318.
14. Wiel C, et al. BACH1 Stabilization by Antioxidants Stimulates Lung Cancer Metastasis. *Cell.* 2019;178(2):330-345.e322.
15. Le Gal K, et al. Antioxidants can increase melanoma metastasis in mice. *Sci Transl Med.* 2015;7(308):308re308.
16. Piskounova E, et al. Oxidative stress inhibits distant metastasis by human melanoma cells. *Nature.* 2015;527(7577):186-191.
17. Jiménez-Valerio G，Casanovas O. Angiogenesis and Metabolism: Entwined for Therapy Resistance. *Trends Cancer.* 2017;3(1):10-18.
18. Jiang L, et al. Bach1-induced suppression of angiogenesis is dependent on the BTB domain. *EBioMedicine.* 2020;51:102617.
19. Jiang L, et al. Bach1 Represses Wnt/β-Catenin Signaling and Angiogenesis. *Circ Res.* 2015;117(4):364-375.
20. Yusoff FM, et al. Bach1 plays an important role in angiogenesis through regulation of oxidative stress. *Microvasc Res.* 2021;134:104126.
21. Knowles HJ, et al. Effect of ascorbate on the activity of hypoxia-inducible factor in cancer cells. *Cancer Res.* 2003;63(8):1764-1768.
22. Cohen B, et al. BACH family members regulate angiogenesis and lymphangiogenesis by modulating VEGFC expression. *Life Sci Alliance.* 2020;3(4).
23. Kitamuro T, et al. Bach1 functions as a hypoxia-inducible repressor for the heme oxygenase-1 gene in human cells. *J Biol Chem.* 2003;278(11):9125-9133.

24. Loboda A, et al. HIF-1 induction attenuates Nrf2-dependent IL-8 expression in human endothelial cells. *Antioxid Redox Signal.* 2009;11(7):1501-1517.
25. Li S, et al. EglN3 hydroxylase stabilizes BIM-EL linking VHL type 2C mutations to pheochromocytoma pathogenesis and chemotherapy resistance. *Proc Natl Acad Sci U S A.* 2019;116(34):16997-17006.
26. Sun J, et al. Heme regulates the dynamic exchange of Bach1 and NF-E2-related factors in the Maf transcription factor network. *Proc Natl Acad Sci U S A.* 2004;101(6):1461-1466.
27. Zenke-Kawasaki Y, et al. Heme induces ubiquitination and degradation of the transcription factor Bach1. *Mol Cell Biol.* 2007;27(19):6962-6971.
28. Sayin VI, et al. Antioxidants accelerate lung cancer progression in mice. *Sci Transl Med.* 2014;6(221):221ra215.
29. Chandel NS, et al. Reactive oxygen species generated at mitochondrial complex III stabilize hypoxia-inducible factor-1alpha during hypoxia: a mechanism of O2 sensing. *J Biol Chem.* 2000;275(33):25130-25138.
30. Hamanaka RB， Chandel NS. Mitochondrial reactive oxygen species regulate hypoxic signaling. *Curr Opin Cell Biol.* 2009;21(6):894-899.
31. Chandel NS, et al. Mitochondrial reactive oxygen species trigger hypoxia-induced transcription. *Proc Natl Acad Sci U S A.* 1998;95(20):11715-11720.
32. Ivan M, et al. Biochemical purification and pharmacological inhibition of a mammalian prolyl hydroxylase acting on hypoxia-inducible factor. *Proc Natl Acad Sci U S A.* 2002;99(21):13459-13464.
33. Maclean A, et al. Fallopian tube epithelial cells express androgen receptor and have a distinct hormonal responsiveness when compared with endometrial epithelium. *Hum Reprod.* 2020;35(9):2097-2106.
34. Dogan S, et al. DNA methylation-based classification of sinonasal undifferentiated carcinoma. *Mod Pathol.* 2019;32(10):1447-1459.

35. Paschalis A, et al. Prostate-specific Membrane Antigen Heterogeneity and DNA Repair Defects in Prostate Cancer. *Eur Urol.* 2019;76(4):469-478.
36. Guo R, et al. MET IHC Is a Poor Screen for MET Amplification or MET Exon 14 Mutations in Lung Adenocarcinomas: Data from a Tri-Institutional Cohort of the Lung Cancer Mutation Consortium. *J Thorac Oncol.* 2019;14(9):1666-1671.
37. Kaya-Okur HS, et al. CUT&Tag for efficient epigenomic profiling of small samples and single cells. *Nat Commun.* 2019;10(1):1930.
38. Langmead B，Salzberg SL. Fast gapped-read alignment with Bowtie 2. *Nat Methods.* 2012;9(4):357-359.
39. Zhang Y, et al. Model-based analysis of ChIP-Seq (MACS). *Genome Biol.* 2008;9(9):R137.
40. Heinz S, et al. Simple combinations of lineage-determining transcription factors prime cis-regulatory elements required for macrophage and B cell identities. *Mol Cell.* 2010;38(4):576-589.
41. Ramírez F, et al. deepTools2: a next generation web server for deep-sequencing data analysis. *Nucleic Acids Res.* 2016;44(W1):W160-165.

Figure 1

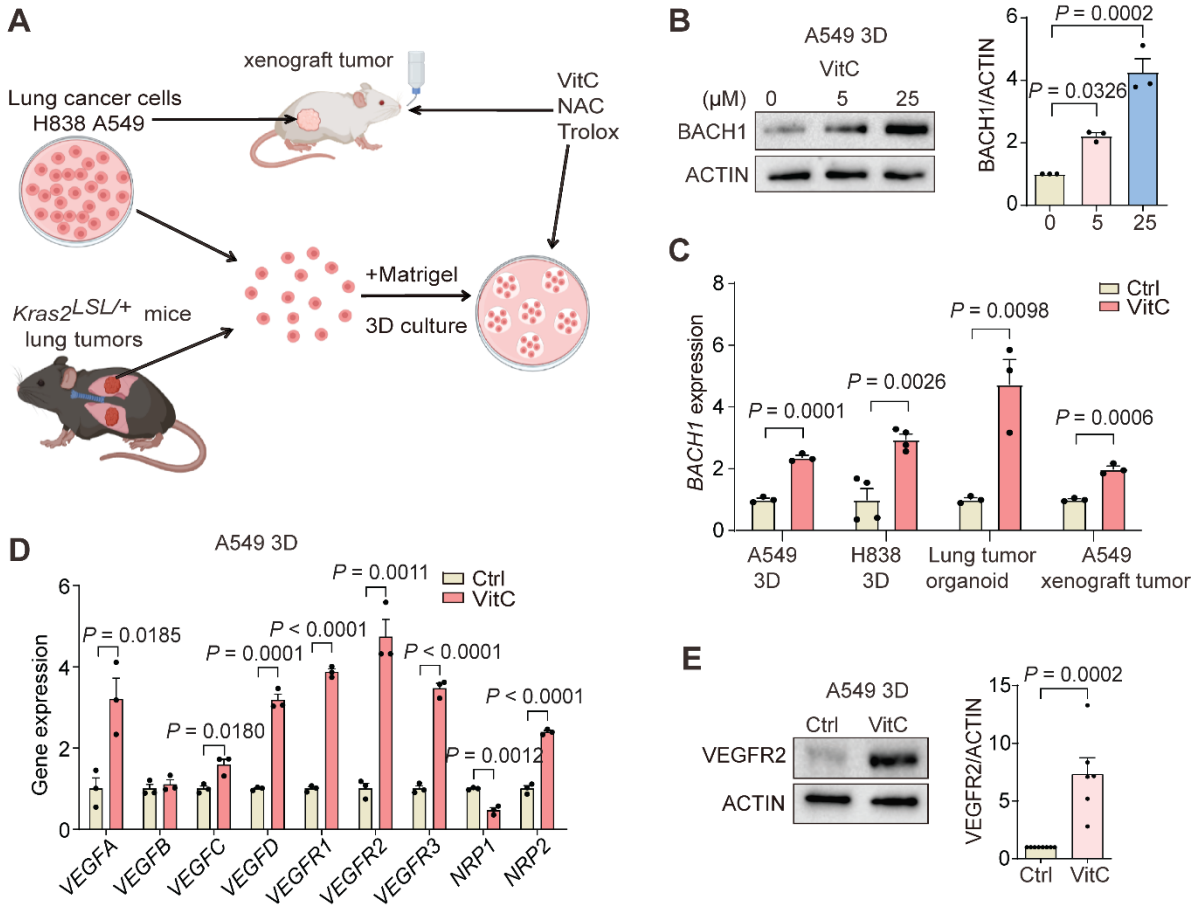

Figure 1. Antioxidants stabilize BACH1 and induce angiogenesis gene expression in non-small cell lung cancer organoids and tumors by upregulating BACH1 expression. (**A**) Experimental design. (**B**) Left, BACH1 protein levels in spheroids incubated 7 days with 25 μM VitC. Right, BACH1 levels by densitometry (n = 3 experiments). (**C**) RT-qPCR of *BACH1* in A549 and H838 spheroids, and lung tumor organoids incubated 7 days with 25 μM VitC; and A549 xenograft tumors from mice administered VitC (3.47 g/l) in the drinking water for 7 weeks (n = 3 experiments). (**D**) RT-qPCR of angiogenesis genes in spheroids incubated with 25 μM VitC for 7 days (n = 3 experiments). (**E**) Left, VEGFR2 protein levels in spheroids incubated 25 μM VitC for 7 days. Right, amounts of VEGFR2 determined by densitometry (n = 6 experiments). Data are mean and SEM. Statistics: Two-tailed unpaired Student's *t* test (panel C, D, E) and one-way ANOVA with Tukey's post-hoc test for multiple comparisons (panel B).

Figure 2

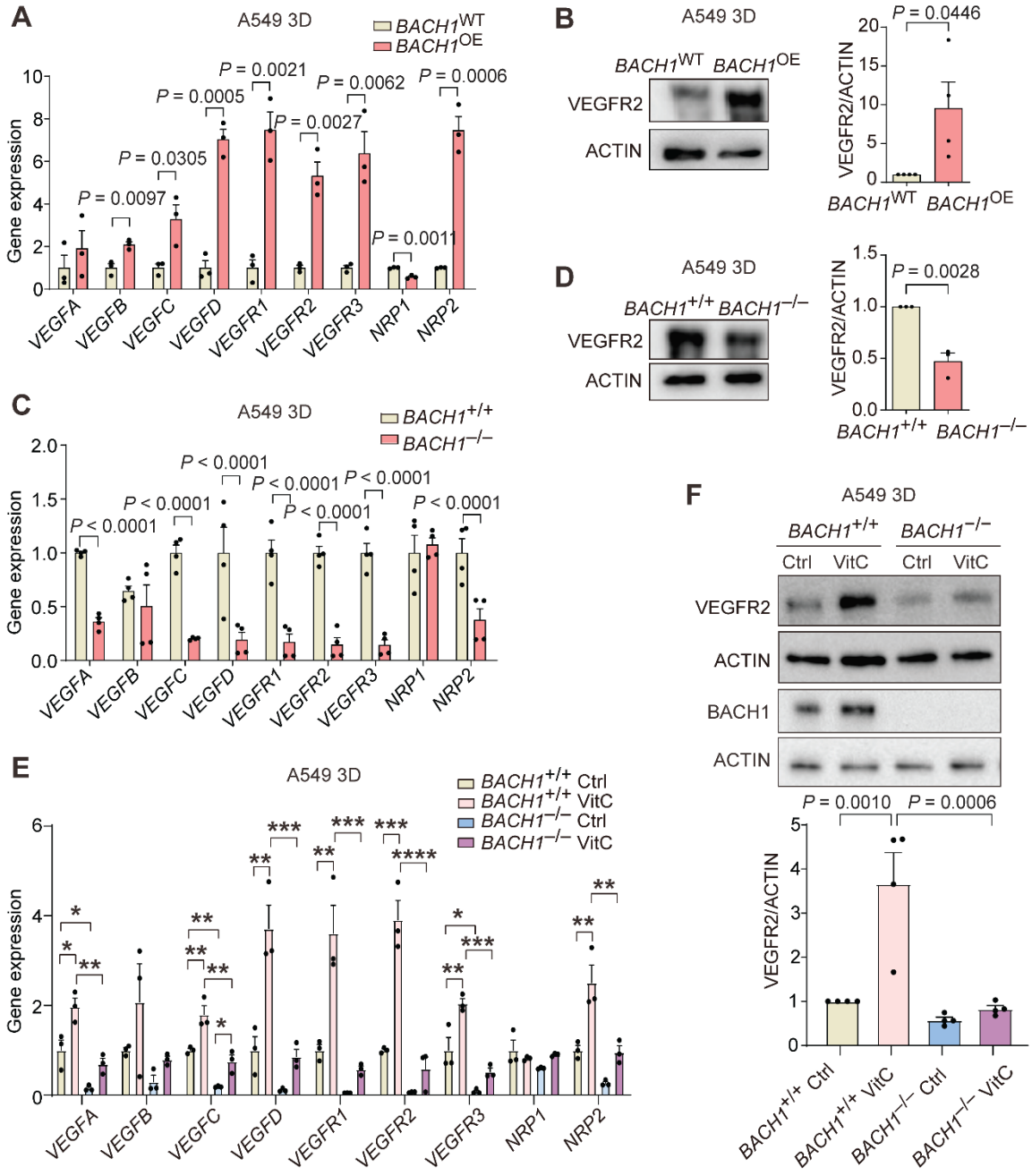

Figure 2. BACH1 controls expression of angiogenesis genes under normoxia. (**A**) RT-qPCR of angiogenesis genes in *BACH1*^{OE} and *BACH1*^{WT} spheroids under normoxia (n = 3 experiments). (**B**) Left, VEGFR2 protein levels in *BACH1*^{OE} and *BACH1*^{WT} spheroids. Right, amounts of VEGFR2 levels (n = 4 experiments). (**C**) RT-qPCR of angiogenesis genes in *BACH1*$^{+/+}$ and *BACH1*$^{-/-}$ spheroids under normoxia (n = 4 experiments). (**D**) Left, VEGFR2 protein levels in *BACH1*$^{+/+}$ and *BACH1*$^{-/-}$ spheroids. Right, VEGFR2 levels (n = 3 experiments). (**E**) RT-qPCR of angiogenesis genes in *BACH1*$^{+/+}$ and *BACH1*$^{-/-}$ spheroids incubated for 7 days with 25 µM VitC or vehicle (Ctrl) (n = 3 experiments). (**F**) Top, VEGFR2 and BACH1 protein levels in *BACH1*$^{+/+}$ and *BACH1*$^{-/-}$ spheroids incubated for 7 days with 25 µM VitC. Bottom, VEGFR2 protein levels (n = 4 experiments). Data are mean and SEM. Statistics: Two-tailed unpaired Student's *t* test (panel A, B, C, D) and one-way ANOVA with Tukey's

post-hoc test for multiple comparisons (panel E, F). * P < 0.05; ** P < 0.01; *** P < 0.005; **** P < 0.001.
.

Figure 3

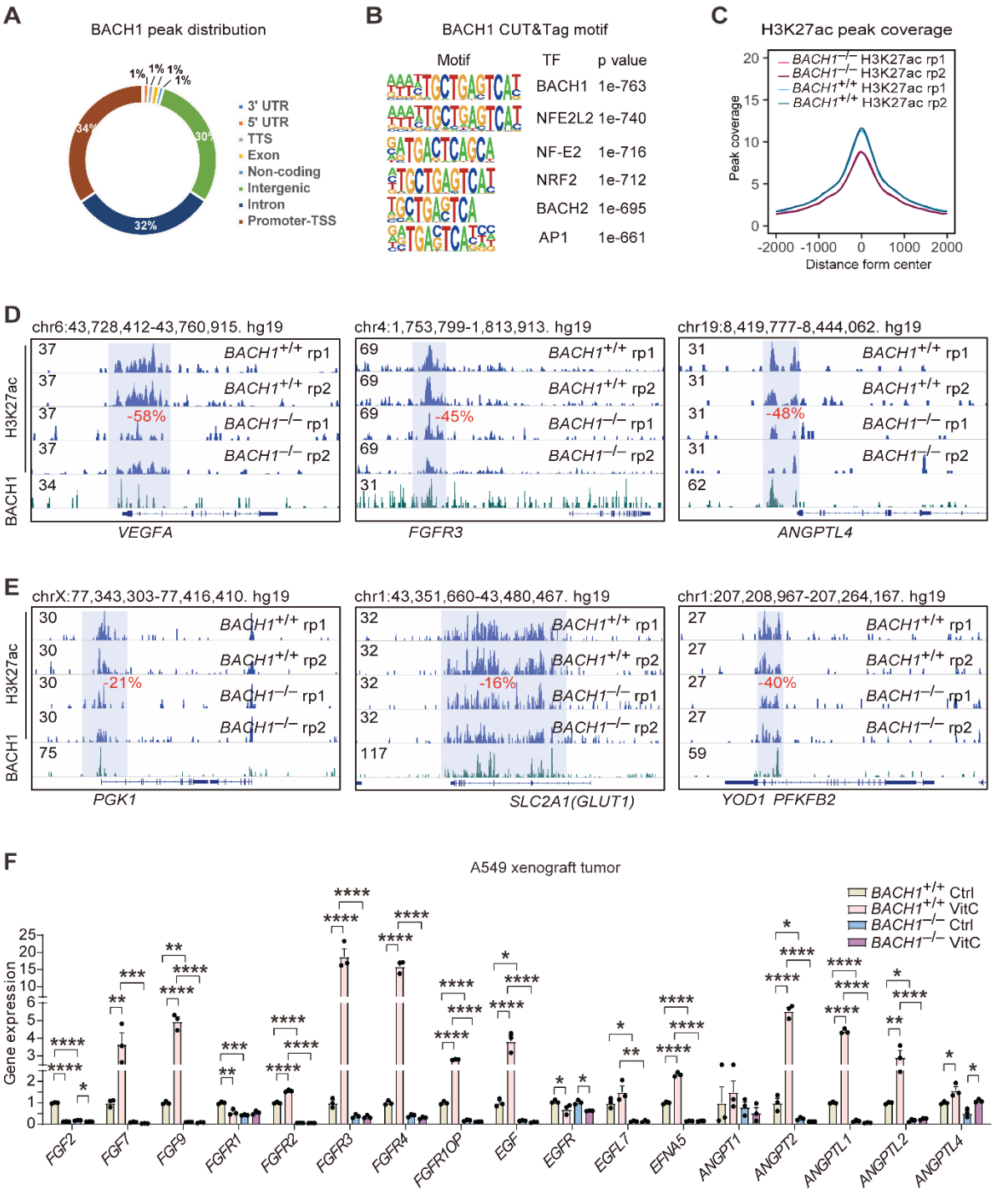

Figure 3. BACH1-mediated expression of angiogenesis and glycolysis genes correlates with BACH1-dependent epigenetic changes at promoter regions. (**A**) Genome-wide profiling of BACH1 chromatin enrichment in A549 spheroids using CUT&Tag. (**B**) Transcription factor DNA-binding motif analysis of BACH1 CUT&Tag peaks. (**C**) Genome-wide plot of H3K27ac peak density in *BACH1*$^{+/+}$ and *BACH1*$^{-/-}$ A549 spheroids; note that the two lines for each genotype replicate (rp1/rp2) overlap. (**D** and **E**) Integrative Genomics Viewer (IGV) tracks showing H3K27ac levels at the indicated angiogenesis (D) and glycolysis (E) gene loci in *BACH1*$^{+/+}$ and *BACH1*$^{-/-}$ A549 spheroids. BACH1 peaks are shown at the bottom to indicate overlap with

H3K27ac-marked regions. Regions with significant H3K27ac changes in *BACH1*$^{-/-}$ compared with *BACH1*$^{+/+}$ A549 spheroids are highlighted in blue; the percent change is indicated with red numbers. (**F**) RT-qPCR of the expression of a broader set of angiogenesis-related genes in tumors of mice engrafted with *BACH1*$^{+/+}$ and *BACH1*$^{-/-}$ A549 lung cancer cells; the mice were given VitC (3.47 g/l) or normal drinking water for 7 weeks (n = 3 experiments). rp, replicate. Data are mean and SEM. Statistics: One-way ANOVA with Tukey's post-hoc test for multiple comparisons (panel F). * $P < 0.05$; ** $P < 0.01$; *** $P < 0.005$; **** $P < 0.001$.

Figure 4

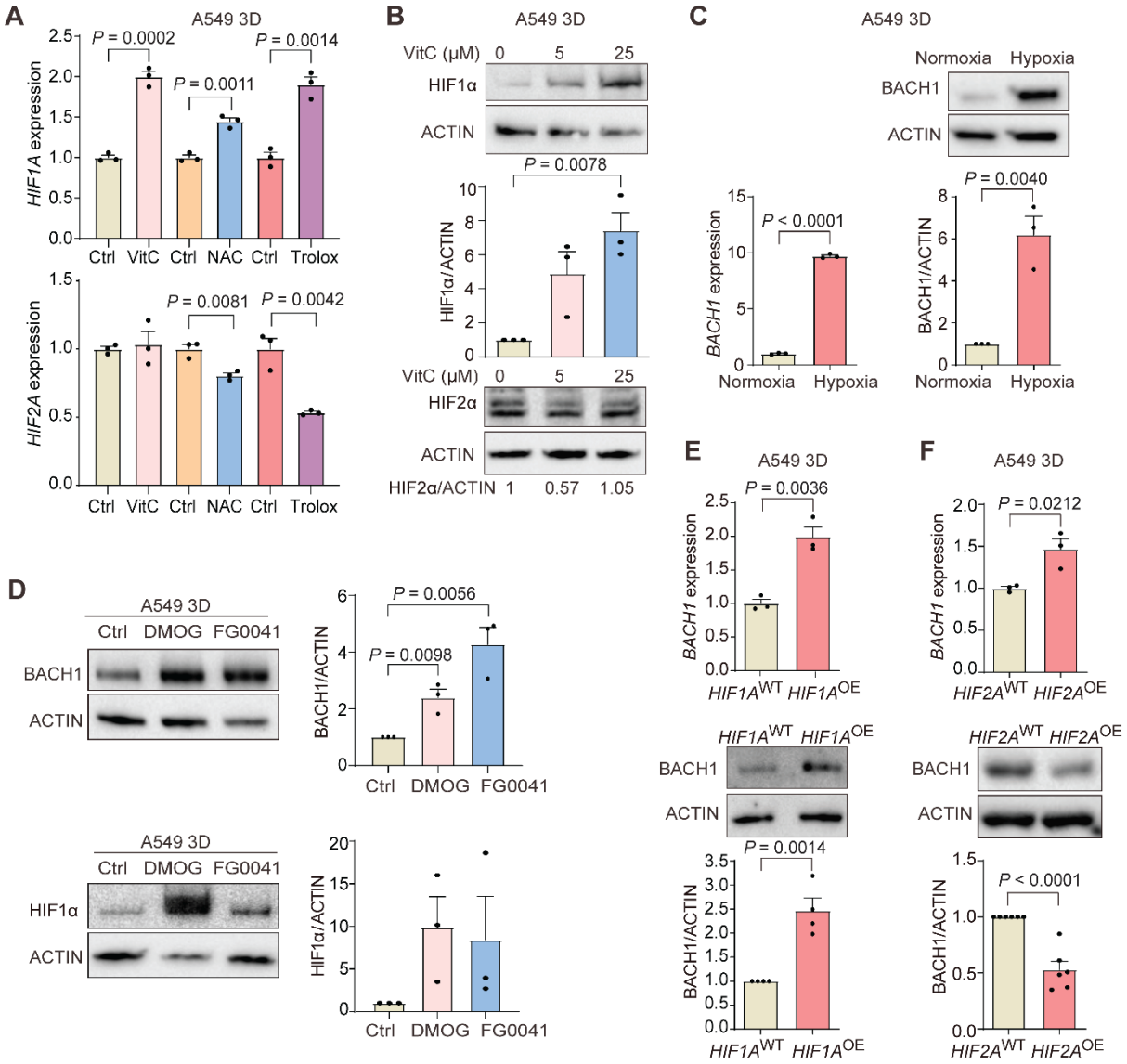

Figure 4. BACH1 expression under normoxia and hypoxia is HIF1α dependent. (**A**) RT-qPCR of *HIF1A* (top) and *HIF2A* (bottom) in spheroids incubated 7 days with antioxidants under normoxia (n = 3 experiments). (**B**) Top, HIF1α in spheroids incubated with VitC. Middle, HIF1α levels by densitometry (n = 3 experiments). Bottom, HIF2α levels. (**C**) Left, RT-qPCR of *BACH1* in spheroids under normoxia (21% O_2) and hypoxia (1% O_2) (n = 3 experiments). Right top, BACH1 levels. Right bottom, BACH1 levels by densitometry (n = 3 experiments). (**D**) Left top, BACH1 in spheroids incubated 16 h with prolyl hydroxylase inhibitors. Right top, BACH1 levels by densitometry (n = 3 experiments). Left bottom, HIF1α protein levels. Right bottom, HIF1α levels by densitometry (n = 3 experiments). (**E**) Top, RT-qPCR of *BACH1* in HIF1α-overexpressing (*HIF1A*^{OE}) and control (*HIF1A*^{WT}) spheroids under normoxia (n = 3 experiments). Middle, BACH1 levels. Bottom, BACH1 levels by densitometry (n = 4 experiments). (**F**) Similar experiments as in panel E using HIF2α-overexpressing (*HIF2A*^{OE}) and control (*HIF2A*^{WT}) spheroids (n = 6 experiments). Data are mean and SEM. Statistics: Two-tailed unpaired Student's *t* test (panel A, C, E, F) and one-way

ANOVA with Tukey's post-hoc test for multiple comparisons (panel B, D). * $P < 0.05$; ** $P < 0.01$; *** $P < 0.005$; **** $P < 0.001$.

Figure 5

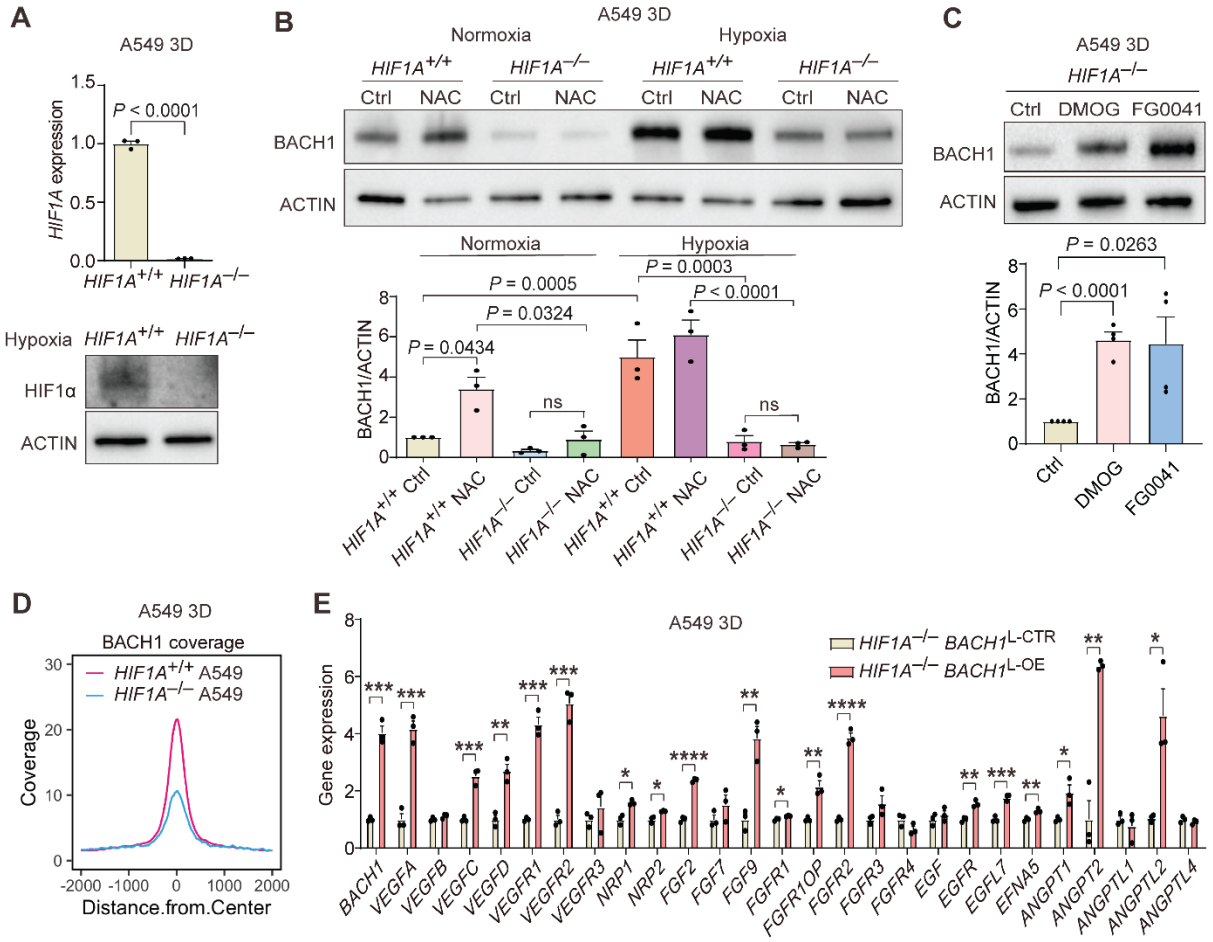

Figure 5. BACH1 increases angiogenesis gene expression in *HIF1A*-deficient lung cancer cells. (**A**) *HIF1A*-knockout validation with RT-qPCR and western blot. (**B**) Top, BACH1 levels in *HIF1A*$^{-/-}$ and *HIF1A*$^{+/+}$ spheroids under normoxia and hypoxia. Bottom, BACH1 levels by densitometry (n = 3 experiments). (**C**) Top, BACH1 in *HIF1A*$^{-/-}$ spheroids incubated 16 hours with prolyl hydroxylase inhibitors. Bottom, BACH1 levels by densitometry (n = 4 experiments). (**D**) Genome-wide BACH1 CUT&Tag peak density plot of *HIF1A*$^{+/+}$ and *HIF1A*$^{-/-}$ spheroids. (**E**) RT-qPCR of *BACH1* and angiogenesis genes in *HIF1A*$^{-/-}$ spheroids with lentiviral BACH1-overexpression (*BACH1*$^{L\text{-}OE}$) and controls (*BACH1*$^{L\text{-}CTR}$) (n = 3 experiments). Data are mean and SEM. Statistics: Two-tailed unpaired Student's *t* test (panel A, E) and one-way ANOVA with Tukey's post-hoc test for multiple comparisons (panel B, C). * P < 0.05; ** P < 0.01; *** P < 0.005; **** P < 0.001.

Figure 6

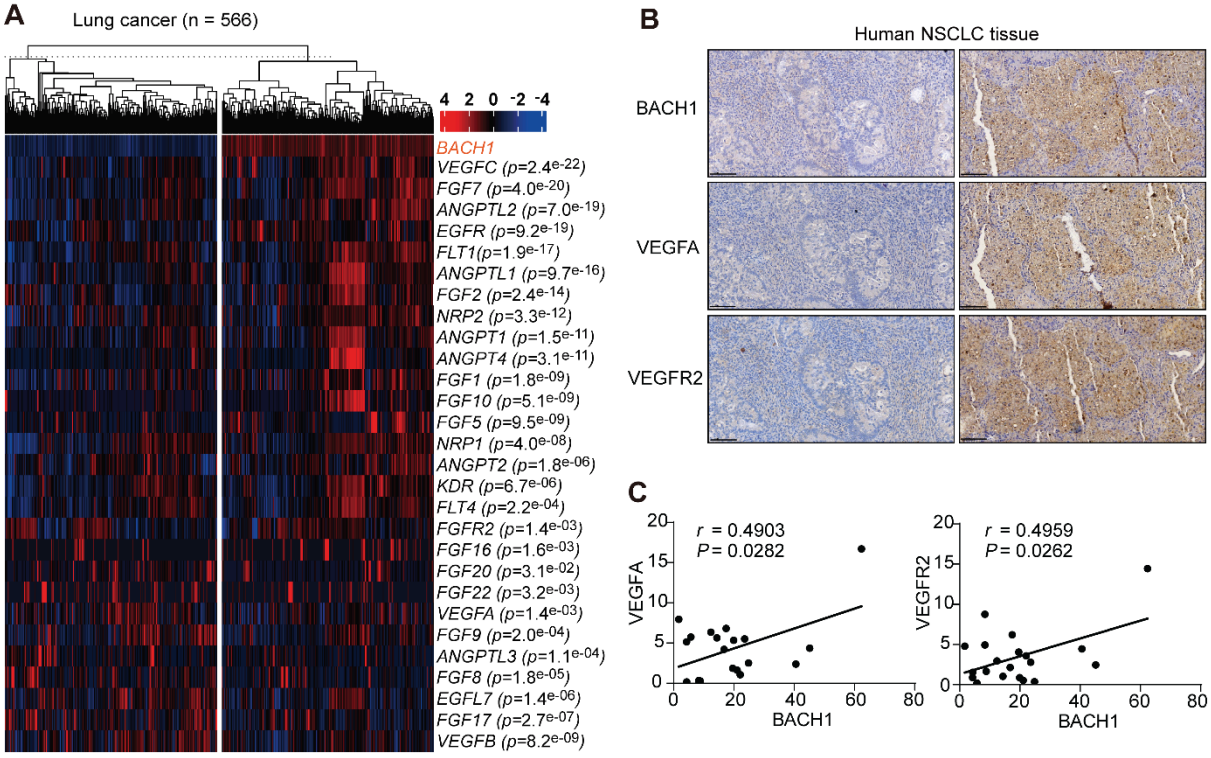

Figure 6. BACH1 expression correlates with angiogenesis gene and protein expression in human NSCLC samples. (**A**) Heat map showing TCGA lung cancer cases with low (left) and high (right) *BACH1* expression. Angiogenic genes whose expression differed significantly between the two groups are listed on the right along with the p value for the correlation with *BACH1* expression. (**B**) Representative immunohistochemical staining of BACH1, VEGFA, and VEGFR2 in consecutive sections of tumors from patients with KRAS-mutant NSCLC; left, tumor sections with low BACH1 expression; right, tumor section with high BACH1 expression. Magnification 20×; scale bar, 100 μm. (**C**) Comparisons of VEGFA (left) and VEGFR2 (right) expression with BACH1 protein expression in human NSCLC tumor sections (n = 20). Data were analyzed using Pearson's correlation test (panel C).

Figure 7

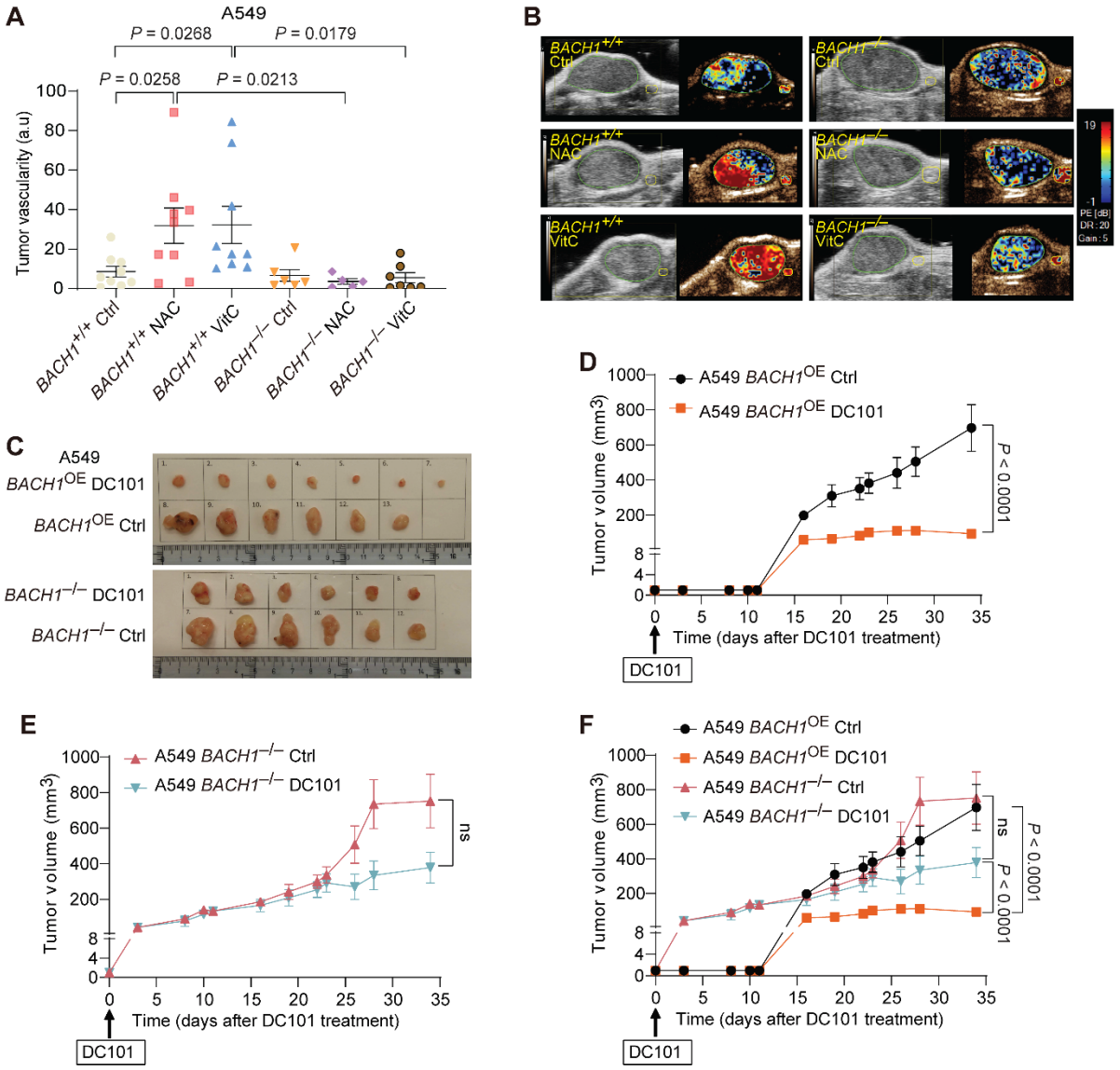

Figure 7. BACH1 increases tumor vascularity and the response to anti-VEGF therapy in xenografts. (**A**) Tumor vascularity (peak enhancement) in *NSG* mice injected s.c. with 5 × 10^5 *BACH1*$^{+/+}$ or *BACH1*$^{–/–}$ A549 cells and administrated water (n = 9 and 6 for +/+ and –/–, respectively), 1 g/l NAC (n = 9 and 5), or 3.47 g/l VitC (n = 9 and 7) for 7 weeks. (**B**) Representative images of tumor vascularity from ultrasound imaging analyses. (**C–E**) Tumor growth in *NSG* mice injected s.c. with 5 × 10^5 *BACH1*^{OE} (C and D) and *BACH1*$^{–/–}$ (C and E) A549 cells. When tumors were palpable, the mice were injected i.p. with PBS (n = 6 in D and E) and 40 mg/kg DC101 (n = 7 and 6 in D and E, respectively) three times a week for five weeks. Tumors were measured three to five times per week. (**i**) Curves from panels D and E shown in the same graph. ns, not significant. Data are mean and SEM. Statistics: one-way ANOVA with Tukey's post-hoc test for multiple comparisons (panel A) and two-way ANOVA with Sidak's post-hoc test for multiple comparisons (panel F).